Exchange and radiative lifetimes for close Frenkel pairs on the zinc sublattice of ZnSe

W. A. Barry* and G. D. Watkins
Department of Physics, Lehigh University, 16 Memorial Drive East, Bethlehem, Pennsylvania 18015
(Received 18 March 1996)

The radiative lifetimes for the individual close Frenkel pairs on the zinc sublattice of ZnSe described in the preceeding paper are measured using optical detection of magnetic resonance. A simple theory is developed for the exchange and radiative lifetimes for deep-donor to deep-acceptor recombination vs pair separation and compared to the lifetime results obtained here and the values for exchange obtained in the preceding paper for the Frenkel pairs. The good agreement obtained allows tentative assignments of the individual pairs to specific lattice sites. [S0163-1829(96)04436-0]

I. INTRODUCTION

In the preceding paper[1] (hereafter referred to as I), twenty-five distinct zinc-interstitial–zinc-vacancy Frenkel pairs of different separations in the ZnSe lattice were observed and studied by electron paramagnetic resonance (EPR) and optically detected magnetic resonance (ODMR), after 1.5–2.5 MeV electron irradiation *in situ* at cryogenic temperatures. In that study, several indicators of lattice separation for the pairs were obtained, including thermal stability, wavelength of luminescence, alignment vs electron beam irradiation direction, and dipole-dipole and exchange interactions between the separated electron on the interstitial and the hole on the vacancy in the excited emitting ODMR state. Specific lattice assignments could be made for two of the closest pairs observed directly by EPR, but for the many more distant ones seen by ODMR, only one tentative ''benchmark'' assignment was attempted. In the absence of a clear unambiguous model for the various indicators of separation, they were simply ordered according to their exchange interaction, which should logically decrease with separation.

In the present paper, we assume the task of making assignments. Our approach is two pronged: (1) We develop an approximate theory for the exchange expected between two separated tightly bound (i.e., *deep*) spin 1/2 particles in a semiconductor. As established in I, this is the case for the Frenkel pairs, and to our knowledge, this important problem has not been addressed previously in the literature. We then test the theory against the tentative benchmark assignment made in I, to determine whether the magnitude of the observed exchange interaction is consistent with the assignment. (2) We present experimental measurements of the radiative lifetimes for several of the pairs. We outline also a theory for the lifetimes vs separation and compare it to the experimental result for the assigned defect separations. With these two separate but related indicators of separation, we then proceed to attempt lattice assignments for all of the observed pairs.

These Frenkel pairs represent a truly unique system in which individual close deep-donor-acceptor pairs are resolved and, via their magnetic resonances, so much detailed information is available concerning their structure and interactions. As such they present a singular opportunity to probe the properties of such defects in semiconductors and to test our understanding of the magnitude and mechanisms for their interactions. In particular, the degree to which we are able to reproduce their exchange and lifetime properties by the theory that we will present not only tests our previous benchmark assignment, but conversely provides an important test of the theory.

The outline of the paper is as follows: In Sec. II, we present a brief outline of the experimental procedures used in the lifetime measurements, referring to I for other relevant details of the EPR and ODMR experiments. In Sec. III A, we develop a theory for the exchange between separated donors and acceptors, first for shallow effective mass states, and then, by extension of the approach, to deep donors and acceptors. In Sec. III B, we show that the results compare favorably with experiment for the benchmark assignment in I, and proceed therefore to tentatively assign the others by comparison with the theory. In Sec. IV A, we develop a similar theory for the radiative lifetimes, first for shallow states and then, again by extension, to deeper states. We include also the spin selection rules which predicts different radiative lifetimes for the dominantly triplet vs singlet spin combinations of the pair. In Sec. IV B, we outline the method for the lifetime measurements and in Sec. IV C, we compare to the experimental results. Again the agreement is very good. In Sec. V, we summarize.

II. EXPERIMENTAL PROCEDURE

The ODMR experiments were performed at 20 GHz in an EPR cryostat modified for *in situ* electron irradiation of the sample at 4.2 K by 2.5 MeV electrons from a Van de Graaff accelerator, with subsequent 1.5 K ODMR detection without intermediate warm up, using fiber optics and a quartz light-pipe for excitation and luminescence collection, respectively. Details of the spectrometer and the samples studied are given in I.

Radiative lifetime measurements for the individual pairs were performed by monitoring the amplitude and phase of the ODMR signal vs frequency of the on-off modulation of the microwaves. The excitation for these experiments was provided by the 476 nm line of an argon laser at a power level of ~ 5 mW. The theory of the measurements and their analysis is given in Sec. IV B. In these measurements, it was necessary to correct for instrumental amplitude and phase

shifts in the optical detection system (North Coast cooled germanium detector-amplifier assembly followed by a lock-in amplifier). For this purpose, a separate calibration of the detection system was performed vs frequency from 2 cps to 200 kcps using an accoustic-optic modulator for on-off modulation of laser excitation applied directly to the detector. In the ODMR lifetime measurements, the phase of the lock-in was adjusted at each frequency to correct for this calibrated phase response, and the in-phase and quadrature output signals were corrected by dividing by the amplitude response.

III. EXCHANGE AND LATTICE ASSIGNMENTS FOR THE FRENKEL PAIRS

A. Theory of exchange

We take the wave function for the excited emitting state of a donor-acceptor pair to be the antisymmetrized product of an electron wave function Ψ_D on the donor, and a hole wave function Ψ_A on the acceptor:

$$\Psi(\mathbf{r}_1,\mathbf{r}_2)=\mathcal{A}[\Psi_D(\mathbf{r}_1)\Psi_A(\mathbf{r}_2)], \tag{1}$$

where $\mathcal{A}$ is the antisymmetry operator and $\mathbf{r}_1$ and $\mathbf{r}_2$ are the coordinates of the two particles. Because of the antisymmetrization, there will be an exchange interaction which can be written as

$$\mathcal{H}=J\mathbf{s}_1\cdot\mathbf{s}_2, \tag{2}$$

between the spins of the two particles, where the dominant contribution to J is given by[2]

$$J=-2\int\int \Psi_D^*(\mathbf{r}_1)\Psi_A^*(\mathbf{r}_2)\frac{e^2}{|\mathbf{r}_1-\mathbf{r}_2|} \times\Psi_D(\mathbf{r}_2)\Psi_A(\mathbf{r}_1)d^3r_1d^3r_2. \tag{3}$$

1. Shallow effective mass states

In the case of shallow effective mass states, we may take

$$\Psi_D(\mathbf{r}_1)\approx\Phi_D(\mathbf{r}_1)u_c(\mathbf{r}_1),$$

$$\Psi_A(\mathbf{r}_2)\approx\Phi_A(\mathbf{r}_2)u_v(\mathbf{r}_2), \tag{4}$$

where Φ_D and Φ_A are slowly varying $1S$-like envelope functions centered on sites separated by $\mathbf{R}$, and u_c and u_v are the Bloch functions at the conduction and valence band edges, respectively. In this case, using the fact that the envelope functions are slowly varying over a unit cell and that the exchange interaction is significant only when the two particles occupy the same unit cell,[3–5] Eq. (3) can be reduced to

$$J\approx-2\Omega_0UJ_0, \tag{5}$$

where

$$J_0=\frac{1}{\Omega_0^2}\int_{\Omega_0}\int_{\Omega_0}u_c^*(\mathbf{r}_1)u_v^*(\mathbf{r}_2)\frac{e^2}{|\mathbf{r}_1-\mathbf{r}_2|} \times u_c(\mathbf{r}_2)u_v(\mathbf{r}_1)d^3r_1d^3r_2, \tag{6}$$

and

$$U=\int|\Phi_D(\mathbf{r})|^2|\Phi_A(\mathbf{r}-\mathbf{R})|^2d^3r. \tag{7}$$

Here, J_0 is the exchange between electron and hole when both are confined to a unit cell, Ω_0 is the volume of a unit cell, and U is the probability density of finding both particles at the same position in space. For hydrogenic $1S$ envelope functions,[4]

$$U=\frac{1}{\pi R(a_A+a_D)^3(\alpha-\beta)^3}\{e^{-2\beta R}[(\alpha^2-\beta^2)\alpha R-2\alpha\beta] +e^{-2\alpha R}[(\alpha^2-\beta^2)(\beta R+2\alpha\beta)]\}, \tag{8}$$

where $\alpha=1/a_A$ and $\beta=1/a_D$, with a_A and a_D, the envelope function Bohr radii for the acceptor and donor, respectively. For $R=0$, U becomes $1/\pi(a_A+a_D)^3$, the value for the free exciton, and Eq. (5) should extrapolate therefore, as $R\rightarrow0$, to the exchange splitting of the free exciton.

The validity of this approach has recently been tested by Cox and Davies[5] for distant shallow-donor to shallow-acceptor recombination in CdS. There, through a clever ODMR study, these workers were able to resolve the exchange splittings and estimate their dependence upon separation. Their results match well the exponential dependence predicted by Eq. (8) for $a_A/a_D\approx0.17$, the value believed appropriate for CdS, and, the extrapolated $R\rightarrow0$ value in their Fig. 11 gives $J=-0.7$ meV, compared to the free exciton value -0.4 meV. (Note that the value quoted by Cox and Davies is for the *exchange splitting* of an $s=1/2$ electron and a $j=3/2$ hole, split by the hexagonal field of the CdS wurtzite lattice, which is $J/2$). Cox and Davies properly worried about this discrepancy, but for our purposes, we consider this good agreement, clearly justifying the approach.

2. Deep Frenkel pair states

Consider now a similar approach for the Frenkel pairs. Even though the electronic states of the constituents are deep and therefore highly localized, an approximation somewhat similar to that of Eq. (4) may still be justified in the spirit of the ''point-ion'' model,[6] successfully used for deep color centers in insulators. The conceptual difference is that u_c and u_v are no longer simple Bloch states at the band edges but rather more atomiclike periodic functions, which in the band model represent sums of Bloch states deeper into the respective bands, and in the point-ion model originate by orthogonalizing the Φ_D and Φ_A envelope functions to the atomic cores. The approximation that the envelope functions are slowly varying over a unit cell, which allowed the separation of the integrals into Eqs. (6) and (7), is clearly much poorer in this case, but again it is not unlike the approximations often successfully employed in the point-ion treatment for hyperfine interactions with distant neighbors of deep defects. Finally, we must point out also that the vacancy envelope wave function may not be simple $1S$-like because the core is a hole primarily in a *p function* on a single Se neighbor of the vacancy.

Keeping these reservations in mind, let us assume that expressions similar to Eqs. (5) and (8) will still apply, but that the value of J_0 may no longer bear a simple relation to that for the free exciton. This departure arises in part directly

from Eq. (6) because of the more localized character of u_c and u_v. In addition, the inadequacy of the various approximations discussed above can also contribute. We will proceed therefore to match our data to Eqs. (5) and (8) with J_0 an adjustable parameter. In so doing, we assume many of the errors introduced by the treatment leading to Eqs. (5) and (8) for such deep defects can be considered to be incorporated into the empirical value determined for J_0.

B. Comparison to experiment and lattice separation assignment

In the preceding paper (I), it was concluded that spectrum labeled X_8, with $|J|=4752$ MHz, arose from the Frenkel pair with the interstitial in a site 14.13 Å in the $\langle 100\rangle$ direction from the vacancy. This is illustrated in Table I, where we have included also the *effective* separation distance of 15.67 Å, taking into account that the hole at the vacancy tends to locate on the Se neighbor which is the most distant from the interstitial. (The sign of J was not determined experimentally in I. In Table I, we have listed the values as negative. This is what would be expected from the treatment in the previous section. In addition, in Sec. IV C, to follow we will present confirming experimental evidence of this assignment. We will therefore take the opportunity now to make this assignment for convenience in the development to follow.) We take for the Bohr radii $a_D=2.05$ Å and $a_A=2.40$ Å, corresponding to the level positions determined in I of $E_C-0.9$ eV and $E_V+0.66$ eV for Zn_i^+ and V_{Zn}^- respectively, as given by Eq. (13) in that reference. With these values, Eq. (8) gives $U=2.38\times10^{-7}$ Å^{-3} at $R=15.67$ Å. With $\Omega_0=45.1$ Å^3, this gives, with Eq. (5), $J_0=2.2\times10^8$ MHz $=0.91$ eV.

Is this a reasonable value? One obvious measure is to compare to experimental estimates for that of the free exciton in ZnSe.[7] Unfortunately, it has proved difficult to extract the small free exciton exchange splitting in ZnSe due to polariton effects, and estimates by different groups differ significantly. For example, estimates by three independent groups[8–10] concluded that the free exciton exchange splitting is $\leqslant 0.1$ meV, corresponding to $|J|\leqslant 0.15$ meV. [They argued that an earlier estimate of 2.0 meV (Ref. 11) involved errors in analysis, and, similarly, that a theoretical treatment[12] that seemed to agree with these earlier values was also in error due to the use of nonorthogonal plane waves in the calculation.[13]] Using this upper limit, with $U=1/\pi(a_{\mathrm{exc}})^3$, where[8] $a_{\mathrm{exc}}=47.2$ Å, Eq. (5) gives for the free exciton, $J_0\leqslant 0.5$ eV. On the other hand, two more recent experiments conclude that $J=-1.2$ meV (Ref. 14) or $J=-1.32$ meV,[15] corresponding to $J_0\approx 5$ eV. In either extreme, however, our value here of 0.9 eV is clearly in the right range, and we conclude therefore that the simple treatment that we have outlined above is leading to reasonable values for the Frenkel pair exchange.

In Table I, we have enumerated all of the zinc-vacancy sites, labeling them by their unit lattice displacements from an interstitial site surrounded by four Se neighbors at (000). Included also for each is the distance between the vacancy and interstitial site, and that between the selenium neighbor of the vacancy that contains the hole and the interstitial site. Using the latter distance as the effective distance R in the exchange interaction, we have calculated J for each site using Eqs. (5) and (8) with $a_D=2.05$ Å, $a_A=2.40$ Å, and $J_0=0.91$ eV and included the results in column four of the table. Finally, in the fifth and sixth columns, we assign the observed spectra by their experimental values of J to the positions with closest predicted value. We include also the closer $S=1$ pairs $(A-D)$, for which the exchange is too large to measure, as well as the close $S=1/2$ $\langle 111\rangle$ pairs seen only by EPR (V^{II}), or by both EPR and ODMR (V^I). For V^I, V^{II}, and $B(V^{III})$, the assignments have already been suggested in I from their alignment properties vs beam orientation. The remaining $A(V^{IV})$, C, and D spectra have been tentatively assigned according to their relative annealing and peak luminescence properties, as given in I. The results are presented in graphical form in Fig. 1.

We note the remarkable fact that the simple treatment outlined above, matching X_8 to the (050) site, appears to account quite well for all but three of the closer sites, one of which, the (001) site, is probably not stable, anyway. Of course the specific assignments of these closer pairs, based here for X_1-X_8 on the assumption of a monotonic decrease of $|J|$ vs separation, could be in error. Superexchange effects and angular dependences associated with non-S-like character of the envelope wave functions could be important and cause irregularities in a simple monotonic radial exchange dependence. Minor inconsistencies with the other indicators of distance (fine structure tensor **D**, annealing temperature, $\lambda_{\max}$) given in Tables IV and V in I suggest this possibility. Another possible irregularity is that ODMR spectra A and D were analyzed to have C_{3v} $\langle 111\rangle$ symmetry but we have been forced to assign them to sites of lower symmetry, the one such site available, (111), already being assigned to V^I. We must conclude that the apparent C_{3v} symmetry in the ODMR reflects primarily the dangling bond $\langle 111\rangle$ character of the isolated vacancy and the slight departures due to the nearby interstitial are not resolved in these cases. Evidence for this is the identification of A in I with the V^{IV} Frenkel pair seen in EPR, which, in the higher EPR resolution, was established to have C_{1h} symmetry, its axial symmetric g tensor being tilted away from the $\langle 111\rangle$ direction by only $\sim 1°$.

Overall, the general agreement must be considered a strong confirmation that this simple approach serves as a reasonable guide to the relationship between exchange and separation and that the lattice site assignments must therefore be approximately correct. The assignments beyond X_8 are considerably less complete, but that is perhaps not unreasonable. Most of the ODMR signals for these more distant pairs would fall in the poorly resolved central spectral region. The specific spectra X_9-X_{20} that were analyzed represented the dominant ones in a sea of weaker less clearly resolved ones, as is evident in Fig. 9 of I, and in some cases could easily represent the unresolved superposition of several separations of comparable exchange.

IV. RADIATIVE LIFETIMES

A. Theory

Like exchange, the radiative lifetime of an individual pair also depends upon the overlap between the electron wave function on the interstitial and the hole wave function on the

TABLE I. Tentative assignment of the observed Frenkel pairs to specific lattice sites, and the measured radiative lifetimes for their singlet and triplet excited states. The available lattice site arrangements are enumerated by giving the lattice position of V_{Zn} as measured from Zn_i in a site surrounded by four seleniums located at (000). ($a=5.66$ Å is the ZnSe cubic unit cell dimension.) The assignments have been made by matching the experimental values of J with those calculated by Eqs. (6) and (8), with $J_0=0.91$ eV and with separation R between Zn_i and the Se neighbor of V_{Zn} containing the hole (Se_V), as given in the third column.

V_{Zn} site $\left(\frac{a}{2},\frac{a}{2},\frac{a}{2}\right)$	$R(V_{Zn}\text{-}Zn_i)$ (Å)	$R(Se_V\text{-}Zn_i)$ (Å)	J(calc.) (MHz)	J (exp.) (MHz)	Frenkel pair	τ_r^{-1}(singlet) (kcps)	τ_r^{-1}(triplet) (kcps)
(001)	2.83	4.68	-12154317				
(11$\bar{1}$)	4.89	6.16	-4865034		V^{II}		
(111)	4.89	7.34	-2229415		V^{I}		
(210)	6.32	8.36	-1105575				
(221)	8.48	10.09	-322130		$A(V^{IV})$		5.0
(30$\bar{0}$)	8.48	10.85	-184800		$B(V^{III})$		22.0
(31$\bar{1}$)	9.37	10.85	-184800		C		10.7
(311)	9.37	11.56	-109261		D		3.3
(32$\bar{0}$)	10.19	12.23	-66206	-57050	X_1		
(32$\bar{2}$)	11.65	12.87	-40855	-32048	X_2		
(410)	11.65	13.47	-25896	-18827	X_3		
(322)	11.65	14.04	-16620	-15382	X_4	116	
(33$\bar{1}$)	12.31	14.05	-16620	-14624	X_5		
(331)	12.31	14.61	-10804	-13823	X_6		
(42$\bar{1}$)	12.95	14.61	-10804	-11833	X_7		12.1
(421)	12.95	15.15	-7117				
(05$\bar{0}$)	14.13	15.67	-4752	-4752	X_8	86.3	9.9
(33$\bar{3}$)	14.68	15.67	-4752				
(40$\bar{3}$)	14.13	16.17	-3217				
(51$\bar{1}$)	14.68	16.17	-3217				
(15$\bar{1}$)	14.68	16.65	-2209	-1964	X_9		
(43$\bar{2}$)	15.21	16.65	-2209	-1820	X_{10}	23.5	7.7
(333)	14.68	17.13	-1517	-1619	X_{11}	24.5	11.4
(250)	15.21	17.13	-1517	-1427	X_{12}	22.8	
(42$\bar{3}$)	15.21	17.59	-1055	-1319	X_{13}	20.9	4.8
(52$\bar{2}$)	16.23	17.59	-1055	-908	X_{14}	10.6	
(414)	16.23	18.03	-746	-719	X_{15}	11.3	6.9
(25$\bar{2}$)	16.23	18.47	-525				
(53$\bar{1}$)	16.71	18.47	-525	-606	X_{16}	8.7	5.9
(351)	16.71	18.90	-375				
(61$\bar{0}$)	17.18	18.90	-375	-420	X_{17}	5.4	3.9
(44$\bar{3}$)	18.09	19.32	-267	-252	X_{18}	4.3	4.0
(62$\bar{1}$)	18.09	19.72	-195				
(53$\bar{3}$)	18.52	19.72	-195				
(261)	18.09	20.13	-141				
(405)	18.09	20.13	-141				
(344)	18.09	20.52	-102	-90	X_{19}	3.0	4.4
(42$\bar{5}$)	18.95	-20.52	-102				
(353)	18.52	20.90	-75				
(360)	18.95	20.90	-75				
(542)	18.95	21.28	-57				
(70$\bar{0}$)	19.78	21.28	-57				
(23$\bar{6}$)	19.78	21.28	-57				
(71$\bar{1}$)	20.17	21.65	-42	-36	X_{20}		
(362)	19.78	22.02	-30				
distant			0	~ 0	distant	0.13	

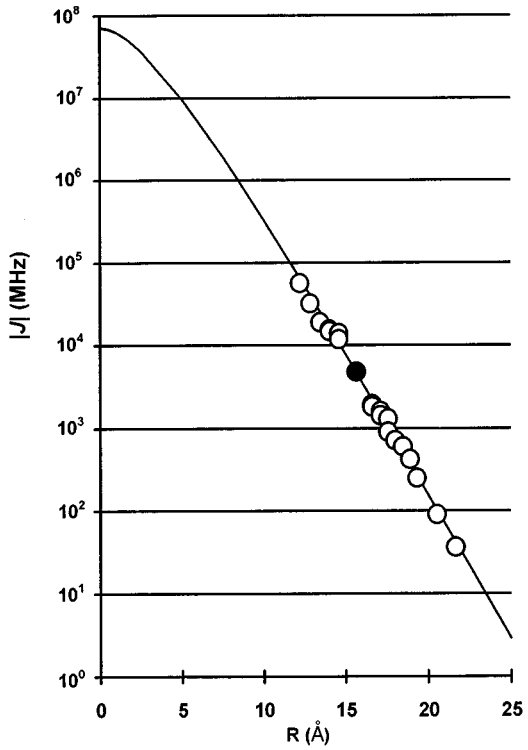

FIG. 1. Assignment of the separation R for the observed Zn_i-V_{Zn} Frenkel pairs according to their experimental values of exchange J. The curve was calculated with $J_0=0.91$ eV, determined by matching the value for X_8, the black point in the figure.

vacancy to which the electron makes the transition. It thus also serves as an independent indicator of separation. The lifetime will also depend on the component of total spin S in the excited state of the combined $s=1/2$ electron and hole particles, since the transition is to a ground $S=0$ state.

Following Dexter,[16] the spontaneous radiative recombination rate between excited (Ψ_e) and ground (Ψ_g) states of a defect in a medium can be written

$$W=\left[\left(\frac{\mathcal{E}_{\rm eff}}{\mathcal{E}_0}\right)^2 n\right]\frac{4\alpha\omega^3}{3c^2}|\langle\Psi_g|\mathbf{r}|\Psi_e\rangle|^2, \tag{9}$$

where α is the fine structure constant, $\hbar\omega$, the energy difference between ground and excited states, c, the velocity of light, and $\mathbf{r}$, the electron position operator. The term in square brackets is due to the presence of the dielectric medium, where $\mathcal{E}_{\rm eff}$ is the effective field seen by the defect, $\mathcal{E}_0$ is the average field in the medium, and n is the index of refraction.

In the case of donor-acceptor recombination, the spatial parts of the excited and ground states can be replaced by Ψ_D and Ψ_A, the occupied interstitial donor and empty vacancy acceptor states, respectively, leading to

$$W=\left[\left(\frac{\mathcal{E}_{\rm eff}}{\mathcal{E}_0}\right)^2 n\right]\frac{4\alpha\omega^3}{3c^2}|\langle\Psi_A|\mathbf{r}|\Psi_D\rangle|^2|\langle\chi_e|\chi_g\rangle|^2, \tag{10}$$

where $|\chi_e\rangle$ and $|\chi_g\rangle$ are the spin functions of the excited and ground states, respectively.

1. Shallow effective mass states

For shallow donor and acceptor states, we may approximate the matrix element of $\mathbf{r}$ above in the identical way in which we treated the exchange integral in the preceeding section. We employ the approximation of Eq. (4) with $r_1=r_2=r$, plus the approximation that the envelope wave functions are slowly varying over a unit cell, allowing separation of the integral over a unit cell from that over the greater extent of the envelope functions, and utilize the orthogonality of u_v and u_c. This leads directly to

$$W\approx\left[\left(\frac{\mathcal{E}_{\rm eff}}{\mathcal{E}_0}\right)^2 n\right]\frac{4\alpha\omega^3}{3c^2}r_0^2 I_{\rm DA}^2|\langle\chi_e|\chi_g\rangle|^2, \tag{11}$$

where

$$r_0^2=\left|\frac{1}{\Omega_0}\int_{\Omega_0} u_c(\mathbf{r})\mathbf{r}u_v(\mathbf{r})d^3r\right|^2, \tag{12}$$

and

$$I_{\rm DA}=\int \Phi_D(\mathbf{r})\Phi_A(\mathbf{r}-\mathbf{R})d^3r. \tag{13}$$

For 1S envelope functions, $I_{\rm DA}$ is given by[17]

$$I_{\rm DA}=\frac{8(\alpha\beta)^{3/2}}{(\alpha^2-\beta^2)^3R}\{[4\alpha\beta+(\alpha^2-\beta^2)\beta R]\exp(-\alpha R) -[4\alpha\beta-(\alpha^2-\beta^2)\alpha R\exp(-\beta R)]\}, \tag{14}$$

where α, β, and R have been defined earlier in Eq. (8).

The dipole matrix element in Eq. (12) may also be expressed in terms of the momentum operator $\mathbf{p}$,[18]

$$\int_{\Omega_0} u_c(\mathbf{r})\mathbf{r}u_v(\mathbf{r})d^3r=\frac{-i}{m\omega_{vc}}\int_{\Omega_0} u_c(\mathbf{r})\mathbf{p}u_v(\mathbf{r})d^3r, \tag{15}$$

leading, for shallow effective mass donor and acceptor states, where u_c and u_v properly represent the states at the band edges, to

$$r_0^2=\frac{\hbar^2E_p}{2mE_g^2}, \tag{16}$$

where E_p is the energy equivalent interband matrix element commonly encountered in $\mathbf{k}\cdot\mathbf{p}$ band structure theory, and defined by[19]

$$E_p=\frac{2}{m}\left|\frac{1}{\Omega_0}\int_{\Omega_0} u_c(\mathbf{r})\mathbf{p}u_v(\mathbf{r})d^3r\right|^2. \tag{17}$$

For shallow donor-acceptor recombination, we expect therefore

$$W\approx\left[\left(\frac{\mathcal{E}_{\rm eff}}{\mathcal{E}_0}\right)^2 n\right]\frac{2\alpha\hbar^2\omega^3E_p}{3mc^2E_g^2}I_{\rm DA}^2|\langle\chi_e|\chi_g\rangle|^2. \tag{18}$$

The work of Cox and Davies[5] in CdS serves also as a check on this treatment in that they also estimated the radiative rates of the shallow-donor-acceptor pairs in a separation range R that overlapped their exchange measurements, giving $W=2\times10^8\ \exp(-2R/a_D)\ \sec^{-1}$. For their studies, $R>a_D>a_A$, and Eq. (14) reduces to

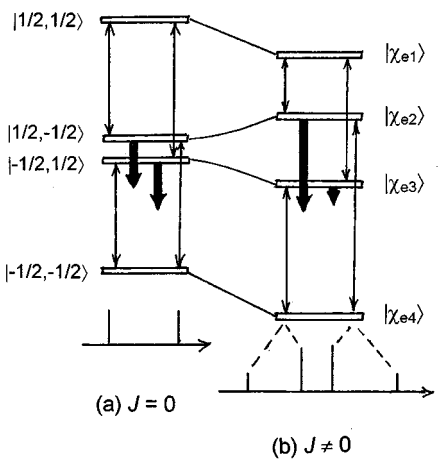

FIG. 2. Zeeman energy diagram for the excited states of a Frenkel pair, (a) without, and (b) with exchange. Shown are the radiative transitions to the ground state (dark arrows) and the ODMR transitions (light arrows). Shown also schematically are the resulting ODMR spectra, the individual V_{Zn}^{-} and Zn_i^{+} lines for $J=0$ each splitting into two lines, the stronger inner ones becoming the allowed transitions within the total $S=1$ manifold, the outer weaker ones the forbidden ones between the $S=0$ and $S=1$ manifolds.

$$I_{\mathrm{DA}}^2 \rightarrow \frac{64(a_A/a_D)^3}{[1-(a_A/a_D)^2]^4}\exp(-2R/a_D), \tag{19}$$

in agreement with the observed dependence on separation. With $\hbar\omega=2.25$ eV for the luminescence,[5] $a_A/a_D=0.17$, $E_g=2.82$ eV, $E_p=24.2$ eV,[19] $\mathcal{E}_{\mathrm{eff}}\approx\mathcal{E}_0$, as expected for extended defects, $n=2.5$, and $|\langle\chi_e|\chi_g\rangle|^2\sim 0.5$ (as we will demonstrate below), Eq. (18) gives, with Eq. (19), 2.2×10^8 sec^{-1} for the preexponential factor, in remarkable agreement. For use later, we note that Eq. (16) gives with these values, $r_0^2=11.8$ Å^2.

2. Deep Frenkel pair states

Again, as for the exchange, we will assume that a similar expression to Eq. (11) applies approximately for the deeper Frenkel pair radiative rates but with r_0^2 no longer necessarily simply related to the band parameters as in Eq. (16). In Sec. IV C, we will describe experimental measurements for the Frenkel pair lifetimes and, assuming the lattice separation assignments of the preceeding section, derive an empirical value for r_0^2 using Eq. (11). A test of the general validity of the approach will again be provided by comparison of the empirical value for r_0^2 with that of Eq. (16).

3. Spin selection rules

For a single Frenkel pair, there are four excited states arising from the $m_e=\pm1/2$ and $m_h=\pm1/2$ spin states of the electron on the interstitial donor and hole on the vacancy, respectively. This is illustrated in Fig. 2(a) without exchange, and in Fig. 2(b) with exchange J. The spin parts of the four excited states of an exchange coupled donor-acceptor pair can be written in terms of the $|m_h,m_e\rangle$ product states of the individual $s=1/2$ spins as

$$|\chi_{e1}\rangle=|1/2,1/2\rangle, \tag{20}$$

$$|\chi_{e2}\rangle=\frac{|1/2,-1/2\rangle+Q|-1/2,1/2\rangle}{\sqrt{1+Q^2}}, \tag{21}$$

$$|\chi_{e3}\rangle=\frac{-Q|1/2,-1/2\rangle+|-1/2,1/2\rangle}{\sqrt{1+Q^2}}, \tag{22}$$

$$|\chi_{e4}\rangle=|-1/2,-1/2\rangle, \tag{23}$$

where

$$Q=\frac{(g_h-g_e)\mu_B B}{J}\left\{\left[1+\frac{J^2}{(g_h-g_e)^2\mu_B^2B^2}\right]^{1/2}-1\right\}. \tag{24}$$

Here, g_e and g_h are the g values for the donor electron and acceptor hole, respectively, μ_B, the Bohr magneton, B, the applied magnetic field, and J, the exchange interaction. The ground $S=0$ state is

$$|\chi_g\rangle=\frac{|1/2,-1/2\rangle-|-1/2,1/2\rangle}{\sqrt{2}}. \tag{25}$$

$|\chi_{e1}\rangle$ and $|\chi_{e4}\rangle$ are the $M_S=\pm1$ states of the pure triplet $S=1$ manifold with

$$|\langle\chi_g|\chi_{e1}\rangle|^2=|\langle\chi_g|\chi_{e4}\rangle|^2=0, \tag{26}$$

and the optical recombination transitions from these states is therefore ''forbidden.'' The other two states are mixtures of the $S=0$ and $S=1$ states, and

$$|\langle\chi_g|\chi_{e2}\rangle|^2=\frac{(1-Q)^2}{2(1+Q^2)}, \tag{27}$$

$$|\langle\chi_g|\chi_{e3}\rangle|^2=\frac{(1+Q)^2}{2(1+Q^2)}. \tag{28}$$

For the distant pairs, where $|J|\ll|g_h-g_e|\mu_B B$, $Q\approx0$, giving $|\langle\chi_g|\chi_{e1}\rangle|^2\approx|\langle\chi_g|\chi_{e3}\rangle|^2\approx1/2$, independent of separation. (This has been used above for the analysis of the distant shallow-donor-acceptor pair results of Cox and Davies.) For the closer pairs, with large negative value for J, the sign chosen in Fig. 2, and with $g_h>g_e$, the case for the Frenkel pairs, $Q\rightarrow-1$, $|\langle\chi_g|\chi_{e2}\rangle|^2\rightarrow1$, and $|\langle\chi_g|\chi_{e3}\rangle|^2\rightarrow0$. Therefore, the lifetime of state 3 increases, as it becomes more triplet in character, and that of state 2 decreases as it becomes more singlet. The crossover in this behavior occurs when $|J|\simeq|g_h-g_e|\mu_B B$. (For a positive J, $Q\rightarrow+1$, and the roles of the two states reverse with state 2 becoming more triplet in character, etc.)

B. Theory of the ODMR lifetime measurements

Each of the four microwave induced $\Delta M_S=\pm1$ transitions, shown in Fig. 2(b), is between a pure triplet state, $|\chi_{e1}\rangle$ or $|\chi_{e4}\rangle$, with a long spin-forbidden radiative lifetime, and a mixed $S=0$ and $S=1$ state, $|\chi_{e3}\rangle$ or $|\chi_{e3}\rangle$, with a shorter spin-allowed radiative lifetime. As a result, the luminescence increases at resonance for each transition as the defects in the longer lifetime ''bottleneck'' state are transfered to the shorter lifetime radiative state, giving rise to the ODMR signal. In Fig. 3, we simplify the problem therefore

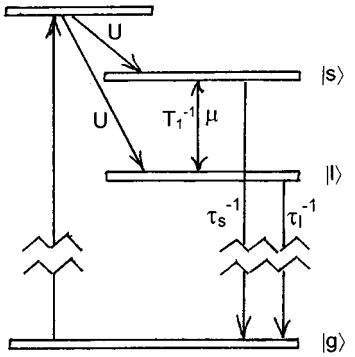

FIG. 3. Equivalent two excited state system treated in the text—one, $|l\rangle$, with a long radiative lifetime, τ_l, the other, $|s\rangle$, with a short radiative lifetime, τ_s. The relevant transitions are indicated.

to that of two excited states — one, $|l\rangle$, with a long radiative lifetime, τ_l, the other, $|s\rangle$, with a short relaxation time, τ_s. As shown, photoexcitation populates each equally at rate U, and microwave induced transitions between the two are induced at rate μ.

The rate equations for the populations N_s and N_l can be written

$$\frac{dN_s}{dt}=\mu(N_l-N_s)+\frac{(N_l-N_s)-(N_l-N_s)_0}{T_1}-\frac{N_s}{\tau_s}+U(N_0-N_s-N_l),$$

$$\frac{dN_l}{dt}=-\mu(N_l-N_s)-\frac{(N_l-N_s)-(N_l-N_s)_0}{T_1}-\frac{N_l}{\tau_l}+U(N_0-N_s-N_l), \tag{29}$$

where μ is the microwave induced transition rate between the two states, T_1 is the spin-lattice relaxation time by which the population difference returns to the thermal equilibrium value $(N_l-N_s)_0$ at a constant population level (N_l+N_s), U is the rate at which the excited states are being generated via laser excitation from the ground state, and N_0 is the total number of the defects.

The luminescence intensity depends upon the populations of the excited states and their radiation rates, giving,

$$I(t)=\frac{N_s}{\tau_s}+\frac{N_l}{\tau_l}. \tag{30}$$

In the ODMR experiment, the microwaves are turned on ($\mu=$ constant) at $t=0$ and off ($\mu=0$) at $t=\pi/\omega_m$ and repeated in square wave fashion at the modulation frequency $\omega_m=2\pi f_m$. The resulting $I(t)$ is sent to a lock-in amplifier, the output of which gives therefore for the ODMR signal,

$$\mathrm{ODMR}=\frac{\omega_m}{2\pi}\int_0^{2\pi/\omega_m}\left[\frac{N_s}{\tau_s}+\frac{N_l}{\tau_l}\right]\sin(\omega_m t+\phi)dt. \tag{31}$$

In our case, the microwave magnetic field in the cavity is estimated to be of the order of several Gauss, giving

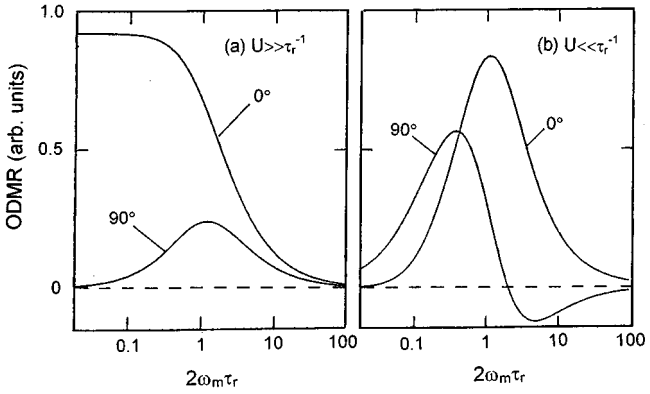

FIG. 4. Modulation frequency dependence of the in-phase (0°) and quadrature (90°) ODMR signals predicted for (a) saturated luminescence, $U\gg\tau_r^{-1}$; and (b) unsaturated, $U\ll\tau_r^{-1}$ with $\tau_s/\tau_l=0.1$.

$\mu\sim10^7\ \mathrm{sec}^{-1}$, much greater than any of the other rates in Eq. (20). To calculate the ODMR signal intensity, we therefore solve Eqs. (29) for $t=0$ to π/ω_m with $\mu=\infty$, and for $t=\pi/\omega_m$ to $2\pi/\omega_m$ with $\mu=0$, match the solutions at the boundaries, and evaluate Eq. (31) for the in-phase ($\phi=0$) and out-of-phase ($\phi=90°$) components. As an additional simplification, we set $T_1=\infty$, justified because its value for isolated V_{Zn}^- has been measured to be[1] ~0.35 sec at $T=1.5$ K, the ODMR measurement temperature, and the value for $\mathrm{Zn}_i{}^+$, being in an S state, should be even longer, both much longer than the radiative times that we will measure. We consider therefore two cases: (a) $U\gg1/\tau_s>1/\tau_l$, corresponding to saturation of the excited states and the luminescence, and (b) $U\ll1/\tau_l<1/\tau_s$, the low excitation, linear case. The results are straight forward and are plotted in Figs. 4(a) and 4(b) for $\tau_s/\tau_l=0.1$. The dependence on the τ_s/τ_l ratio is illustrated in Fig. 5 for the unsaturated case, which will turn out to be the case of interest in our measurements. From it, we see that the peak in the in-phase component, or the zero in the out-of-phase component occurs when

$$2\omega_{\max}\approx\left(\frac{1}{\tau_s}+\frac{1}{\tau_l}\right)\equiv\frac{1}{\tau_r}, \tag{32}$$

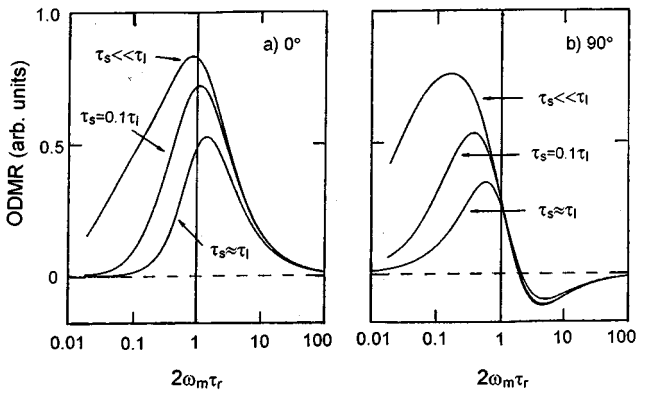

FIG. 5. Dependence of the (a) in-phase (0°), and (b) out-of-phase (90°) ODMR response on τ_s/τ_l, for the unsaturated case, $U\ll\tau_r^{-1}$.

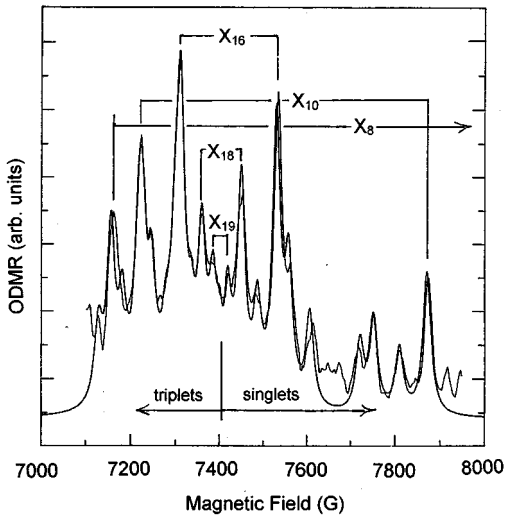

FIG. 6. Least squares fit (heavy line) to the in-phase ODMR central region spectrum (light line) at 1 kHz modulation frequency. Shown is the high field half of the spectrum which is centered around the position for the isolated Zn_i^+ resonance, the signals to lower field becoming ''allowed'' transitions within the triplet manifold, the signals to higher field becoming the ''forbidden'' ones between the singlet and triplet manifold. Some of the dominant pairs are indicated.

serving as a direct measure of what we define as an ''effective'' radiative recombination rate $1/\tau_r$.

C. Experimental results

As illustrated in Fig. 9 of I, the ODMR spectra associated with the more distant pairs behave differently vs modulation frequency, reflecting their different radiative lifetimes, and allowing their separation and analysis in I from an otherwise unresolved superposition of the many pairs which have transitions in the central region of the ODMR spectrum. Some of the spectral lines of the closer pairs also contribute in this region. To extract the radiative lifetimes of each, the in-phase ODMR spectra were recorded at a sequence of modulation frequencies and at each frequency, the intensities of the lines for each identified defect were allowed to vary for best least square fit to the overall spectrum. An example of the fit is shown in Fig. 6, for the high field side of the in-phase ODMR central spectrum at a modulation frequency of 1 kcps. [Each Frenkel pair has four resonances, two on either side of that for the isolated vacancy, and two on either side of that for the isolated interstitial. The intensity of each line present in the spectrum (only the inner lines were observed for the some of the closer pairs) was allowed to vary independently.] The ODMR intensities were then plotted vs modulation frequency for each transition, and the lifetime τ_r estimated.

An alternative method was also used for some of the spectra which were well resolved from the central region, or for the strong $S=1$ close pairs in the central region. For them, the magnetic field was held fixed at the resonance position, and the intensity of the resonance was monitored directly vs modulation frequency. To discriminate against background contributions, a similar study with the magnetic field detuned

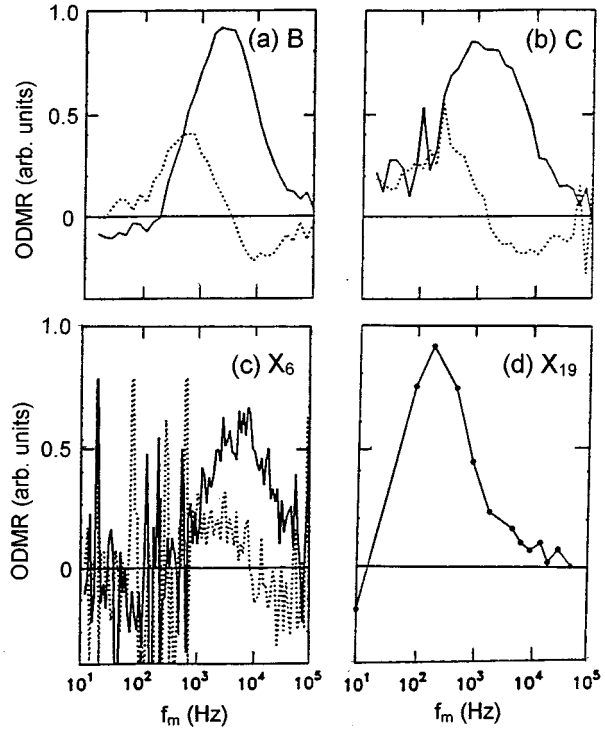

FIG. 7. Modulation frequency responses (in-phase, solid lines; out-of-phase, dotted lines) of some of the Frenkel pairs. (a), (b), and (c) were determined by separately monitoring each resolved ODMR signal. (d) was determined by the least squares method illustrated in Fig. 6.

slightly off resonance was performed and subtracted in each case. Again, τ_r was estimated for each transition from its in-phase and quadrature intensity vs modulation frequency.

In Fig. 7, a few representative examples of the observed modulation frequency dependences are shown, ranging from weak (c) to strong (a) ODMR signals. For these, and all of the others, the in-phase signals were observed to be small at low modulation frequencies, to go through a maximum, and to decrease again at high frequencies. This is characteristic of the unsaturated case, and we therefore estimate τ_r for each ODMR signal from the peak of its in-phase signal, using Eq. (32). We find that, within the accuracy of the measurements, the two inner ODMR transitions, which correspond to transitions from the $|\chi_{e3}\rangle$ state, display the same lifetime, as do the outer transitions, from the $|\chi_{e2}\rangle$ state, with the latter having the shorter lifetime. This is as expected from Eqs. (27) and (28), the $|\chi_{e3}\rangle$ state approaching dominant triplet composition, and $|\chi_{e2}\rangle$, singlet, as $|J|$ increases. We note also that all four ODMR transitions are positive for each defect (produce increase in luminescence), and of approximately equal intensity. This confirms our assumption in the previous section, leading to Eq. (32), that T_1 is long with respect to the radiative lifetimes. If T_1 were comparable, the intensities of the two inner transitions would differ significantly, as would the two outer ones, and if T_1 were shorter, the pair in each case would have opposite signs. In fact, in Fig. 8 of I, the higher field transitions do appear slightly weaker than the corresponding low field transitions of the resolved outer set, which is evidence for weak but not completely negligible relaxation and a *negative* sign for J. (This

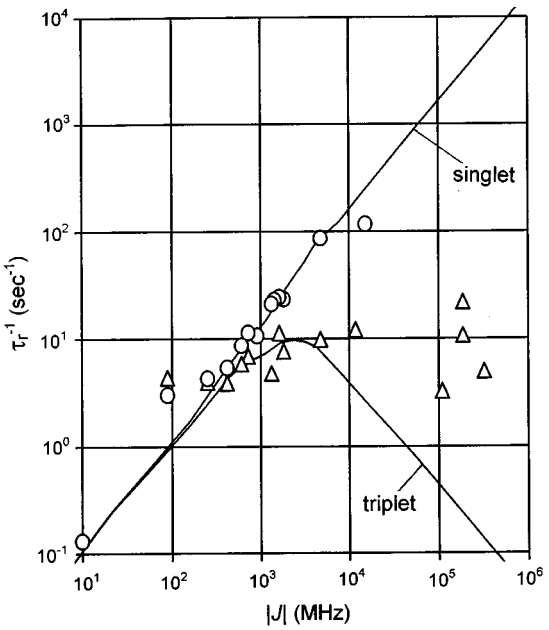

FIG. 8. Radiative lifetime, τ_r^{-1} vs exchange, $|J|$ for the triplet ($\triangle$) and singlet (O) Frenkel pair excited states. The solid curve is calculated, see text.

can be deduced directly from Fig. 10 of I, which predicts the high field components to give negative signals if thermal equilibrium populations exist, because they cause transitions out of a thermally favored radiative state into the bottleneck triplet states. Reversing the sign of J reverses the argument.) This serves to confirm our assignment in Table I of negative values for J.

We include in Table I, the estimated recombination rates (τ_r^{-1}) for each Frenkel pair for which it was possible to perform reliable measurements. The rate, labeled singlet, is the average of the measurements for the two outer transitions (arising from the $|\chi_{e2}\rangle$ predominately singlet state in Fig. 2), and that, labeled triplet, is the average of the two inner transitions (arising from the $|\chi_{e3}\rangle$ predominately triplet state). In Fig. 8, the results are presented in a log-log plot vs $|J|$ for each pair, illustrating a roughly linear relationship for the singlet rates, but a saturation onset for the triplet rates at $|J|\sim 0.5$ cm^{-1}. (The values for the A, B, C, and D, $S=1$ spectra have been plotted at the positions of their calculated exchange values in Table I, and the ''distant'' pair value has been plotted at $J\approx 10$ MHz, consistent with the width of the corresponding ''isolated'' V_{Zn}^{-} and $\mathrm{Zn_i}^{+}$ lines.)

As a test of the theory developed above, we consider the results for X_8, with $J=-4752$ MHz, which has been assigned to the (050) site at $R=15.67$ Å. With $a_D=2.05$ Å, $a_A=2.40$ Å, and $R=15.67$ Å, Eq. (14) gives $I_{\mathrm{DA}}^2=4.5\times 10^{-4}$. Using this, with $\hbar\omega=1.24$ eV, $\mathcal{E}_{\mathrm{eff}}/\mathcal{E}_o\approx 1$, $n=2.5$, and $|\langle\chi_g|\chi_{e2}\rangle|^2\approx 1$ in Eq. (11), and equating to the experimentally observed singlet rate in Table I, we obtain an empirical value for r_0^2 of 10.5 Å^2, in remarkable agreement with the effective mass value of 11.8 Å^2, determined from Eq. (16) in Sec. IV A. Again the close agreement is an unexpected result, and undoubtably somewhat fortuitous, but it clearly again must be considered strong justification of the general treatment that we have presented and, in particular, for the lattice assignments that we have made.

With this empirical value for r_0^2, and the empirical value for $J_0=0.91$ eV determined in Sec. III B, we may now calculate the ratio of the emission rates to exchange vs the separation R, for the Frenkel pairs using Eqs. (5), (8), (11), (14), (24), (27), and (28). The results are plotted in Fig. 8, and the general agreement is clearly good. We note that the experimental results for transitions from the triplet states break away from those from the singlet states precisely as predicted, the ratio of their recombination rates to that of the singlets decreasing steadily beyond the point where $|J|\sim|(g_h-g_e)|\mu_B B$. (They do not actually decrease significantly, however, as the exchange increases, as predicted in our simple model. This suggests that other weaker selection rule violation mechanisms, not considered in our treatment, may be becoming important for these closer triplet pairs.)

V. SUMMARY

We have presented simple theories for the exchange and radiative lifetimes of separated shallow-donor–shallow-acceptor pairs, and have outlined an extension of the approach to treat deep-donor–deep-acceptor pairs, as is the case for the zinc-vacancy–zinc-interstitial Frenkel pairs in ZnSe. The results for exchange have been found to agree satisfactorily with a tentative assignment for one of the Frenkel pairs in I, serving to confirm it and to allow therefore assignments for the other pairs. We have measured the radiative lifetimes of many of the individual pairs and find here too remarkable agreement with the theory. We conclude, therefore, that we are observing most of the closest pairs, and that the simple theory provides a reasonable description of the exchange and radiative lifetime vs separation.

Our results clearly demonstrate that the primary mechanism for the spin dependence of the recombination is that resulting from the ''bottleneck'' of the triplet components of the combined distant Frenkel pair partners. This model has often been cited in the past for distant donor-acceptor recombination, but we believe the present work represents the first unambiguous demonstration that it is correct, and that it applies even for the most distant pairs for which the exchange coupling is extremely weak. It has been possible here because in this truly unique system, the individual pairs are well resolved and the lifetimes of the triplet and singlet components could be separately measured.

ACKNOWLEDGMENTS

This research has been supported jointly by the National Science Foundation under Grant Nos. DMR-89-02572 and DMR-92-04114, and the Office of Naval Research Electronics and Solid State Program under Grant Nos. N00014-90-J-1264 and N00014-94-I-0117.

*Present address: Department of Physics, Oregon State University, Corvalis, OR 97330.

[1] G. D. Watkins, C. F. Rong, W. A. Barry, and J. F. Donegan, Phys. Rev. B **54**, 7779 (1996), preceding paper.

[2] In a Heitler-London treatment such as this, there is another often important term, involving Coulomb interactions between the electrons and the central cores of the two atoms (or defects, as in our case), making up the molecule, see J. H. Van Vleck, Rev. Mod. Phys. **7**, 156 (1935). This term is expected to be small in the case of donor-acceptor states because of the opposite signs of the cores, and is universally neglected. Note also the negative sign in Eq. (3) which differs from definitions in many references. The negative sign is required here because of our definition in Eq. (2), which is the sign convention most often used for the exchange interaction in EPR studies, and which has been adopted in I.

[3] R. J. Elliot, in *Polarons and Excitons*, edited by C. G. Kuper and G. D. Whitfield (Oliver and Boyd, Edinburgh, 1963), p. 269.

[4] F. Thuselt and K. Unger, Phys. Status Solidi B **79**, K39 (1977).

[5] R. T. Cox and J. J. Davies, Phys. Rev. B **34**, 8591 (1986).

[6] B. S. Gourary and F. J. Adrian, in *Solid State Physics: Advances in Research and Applications*, edited by F. Seitz and D. Turnbull (Academic Press, New York, 1960), Vol. 10, p. 127.

[7] For the free exciton, an $s=1/2$ electron is coupled to a $j=3/2$ hole. In the zinc blende ZnSe lattice, the splitting between the resulting $J_{ex}=2$ and $J_{ex}=1$ exciton states is $\frac{2}{3}J$, where J, defined in Eq. (2) in terms of the spins of the two particles, arises from the short range components of the exchange interaction. There are also long range components, not of interest to us, which produce a complicating polariton splitting of the $J=1$ states.

[8] H. Venghaus, Phys. Rev. B **19**, 3071 (1979).

[9] Y. Nozue, M. Itoh, and K. Cho, J. Phys. Soc. Jpn. **50**, 889 (1981).

[10] B. Sermage and G. Fishman, Phys. Rev. B **23**, 5107 (1981).

[11] D. W. Langer, R. N. Euwema, K. Era, and T. Koda, Phys. Rev. B **2**, 4005 (1970).

[12] P. G. Rohner, Phys. Rev. B **3**, 433 (1971).

[13] O. Schütz and J. Treusch, Solid State Commun. **13**, 1155 (1973).

[14] H. Mayer, U. Rössler, S. Permogorov, H. Stolz, H. Vogelsang, and W. von der Osten, J. Cryst. Growth **138**, 195 (1994).

[15] D. Fröhlich, W. Nieswand, U. W. Pohl, and J. Wrzesinski, Phys. Rev. B **52**, 14 652 (1995).

[16] D. L. Dexter, in *Solid State Physics: Advances in Research and Applications*, edited by F. Seitz and D. Turnbull (Academic Press, New York, 1958), Vol. 6, p. 361.

[17] A. T. Vink, J. Lumin. **9**, 159 (1974).

[18] M. Weissbluth, *Atoms and Molecules* (Academic Press, New York, 1978), p. 494.

[19] P. Lawaetz, Phys. Rev. B **4**, 3460 (1971).